CONVECTIVE HEAT TRANSFER AND FLOW STABILITY IN ROTATING DISK CVD REACTORS

William S. Winters and Greg H. Evans
Computational Reactive Processes Department
Sandia National Laboratories
P.O. Box 969
Livermore, California 94551-0969
USA

Ralph Greif
Mechanical Engineering Department
University of California
Berkeley, California 94720-1740
USA

ABSTRACT

The flow and heat transfer of NH_3 and He have been studied in a rotating disk system with applications to chemical vapor deposition reactors. Influence of the important operating parameters were studied numerically over ranges of the primary dimensionless variables: the spin Reynolds number, Re_ω, the disk mixed convection parameter, MCP_d and a new parameter, the wall mixed convection parameter, MCP_w. Inlet velocities were set to the corresponding infinite rotating disk asymptotic velocity. Results were obtained primarily for NH_3. Results show that increasing Re_ω from 314.5 to 3145 increases the uniformity of the rotating disk heat flux and results in thinner thermal boundary layers at the disk surface. At $Re_\omega = 314.5$, increasing MCP_d to 15 leads to significant departure from the infinite disk result with nonuniform disk heat fluxes and recirculating flow patterns. At $Re_\omega = 3145$, the results are closer to the infinite disk for MCP_d up to 15. For large values of MCP_w, the flow recirculates and there is significant deviation from the infinite disk result. The influence of MCP_w on flow stability is increased at larger MCP_d and lower Re_ω. The results show that because of variable transport properties, the flow of NH_3 is less stable than that of He as MCP_d is increased for $MCP_w = 0$ and $Re_\omega = 314.5$.

INTRODUCTION

The chemical vapor deposition (CVD) process is widely used for growing epitaxial layers on heated substrates. The uniformity of layers grown often depends on a stable, uniform and continuous flow of reacting species to the growth surface.

Deviations from the ideal flow behavior in a CVD reactor may result from the effects of variable properties, reactor geometry, gas flow rates, thermal boundary conditions, and variations in gas composition at the reactor inlet. Previous studies by Evans and Greif (1987),

Patnaik *et al.* (1989), and Chou and Gong (1994) have examined these effects for a single component gas in a RDR. Palmateer *et al.* (1987) and Winters *et al.* (1997) have examined convective instabilities under isothermal conditions resulting from binary gas mixing at the reactor inlet.

The present work examines the effects of gas properties and reactor wall temperature; a new parameter for characterizing RDR flows is introduced, namely, a wall mixed convection parameter, MCP_w. In addition, the effects of variable transport properties is shown by comparing results obtained for He and NH_3 gas flows. Results are presented in terms of common RDR flow parameters including the spin Reynolds number, Re_ω, and the disk mixed convection parameter MCP_d. The wall mixed convection parameter, MCP_w, is varied to study the effect of reactor wall temperature on flow stability and convective heat transfer. The reactor performance is quantified by examining radial variations in the disk heat flux, normalized by the ideal infinite rotating disk heat flux (see *e.g.* Evans and Greif (1988)).

MODEL

A cylindrical reactor of radius $\bar{r}_o$ and height $\overline{H}$ contains a spinning disk of radius $\bar{r}_d$ located a distance $\bar{h}$ from the top inlet (*cf.* Fig. 1). The incoming flow consists of a single component ideal gas, either NH_3 or He, with a uniform inlet velocity, $\bar{u}_{in}$.

The dimensionless, steady, variable property, cylindrical, axisymmetric conservation equations of mass, momentum and energy for low Mach number flow, neglecting viscous dissipation and Dp/Dt (pressure work) in the energy equation, are:

$$\frac{1}{r}\frac{\partial(r\rho v)}{\partial r} + \frac{\partial(\rho u)}{\partial x} = 0 \qquad (1)$$

DISCLAIMER

$$\frac{1}{r}\frac{\partial}{\partial r}\left(r\rho vu - \frac{r\mu}{\mathrm{Re}_\omega}\frac{\partial u}{\partial r}\right) + \frac{\partial}{\partial x}\left(\rho uu - \mu\frac{\partial u}{\partial x}\right) =$$

$$-\frac{\partial p_m}{\partial x} + \frac{\mathrm{Gr_d}}{\mathrm{Re}_\omega^{3/2}}\frac{\rho_d}{(1-\rho_d)}(1-\rho) + \frac{1}{r}\frac{\partial}{\partial r}\left(r\mu\frac{\partial v}{\partial x}\right) +$$

$$\frac{\partial}{\partial x}\left\{\mu\frac{\partial u}{\partial x} - \frac{2\mu}{3}\left[\frac{1}{r}\frac{\partial(rv)}{\partial r} + \frac{\partial u}{\partial x}\right]\right\} \qquad (2)$$

$$\frac{1}{r}\frac{\partial}{\partial r}\left(r\rho vv - \frac{r\mu}{\mathrm{Re}_\omega}\frac{\partial v}{\partial r}\right) + \frac{\partial}{\partial x}\left(\rho uv - \mu\frac{\partial v}{\partial x}\right) =$$

$$-\frac{1}{\mathrm{Re}_\omega}\frac{\partial p_m}{\partial r} + r\rho f^2 + \frac{1}{\mathrm{Re}_\omega}\frac{1}{r}\frac{\partial}{\partial r}\left\{r\mu\left[\frac{\partial v}{\partial r} - \right.\right.$$

$$\frac{2}{3}\left.\left(\frac{1}{r}\frac{\partial(rv)}{\partial r} + \frac{\partial u}{\partial x}\right)\right]\right\} - \frac{1}{\mathrm{Re}_\omega}\frac{\mu}{r}\left\{\frac{2v}{r} - \frac{2}{3}\left[\frac{1}{r}\frac{\partial(rv)}{\partial r}\right.\right.$$

$$+ \left.\left.\frac{\partial u}{\partial x}\right]\right\} + \frac{1}{\mathrm{Re}_\omega}\frac{\partial}{\partial x}\left(\mu\frac{\partial u}{\partial r}\right) \qquad (3)$$

$$\frac{1}{r}\frac{\partial}{\partial r}\left(r\rho vf - \frac{r\mu}{\mathrm{Re}_\omega}\frac{\partial f}{\partial r}\right) + \frac{\partial}{\partial x}\left(\rho uf - \mu\frac{\partial f}{\partial x}\right) =$$

$$-\frac{2\rho vf}{r} + \frac{1}{\mathrm{Re}_\omega}\frac{2\mu}{r}\frac{\partial f}{\partial r} \qquad (4)$$

$$\frac{1}{r}\frac{\partial}{\partial r}\left(r\rho vT - \frac{rk}{c_p\,\mathrm{Re}_\omega\,\mathrm{Pr}}\frac{\partial T}{\partial r}\right) + \frac{\partial}{\partial x}\left(\rho uT - \right.$$

$$\left.\frac{k}{c_p\,\mathrm{Pr}}\frac{\partial T}{\partial x}\right) = \frac{k}{c_p^2\,\mathrm{Pr}}\left[\frac{1}{\mathrm{Re}_\omega}\frac{\partial T}{\partial r}\frac{\partial c_p}{\partial r} + \frac{\partial T}{\partial x}\frac{\partial c_p}{\partial x}\right] \qquad (5)$$

where $f \equiv w/r$ in equation (4); u, v, w are the dimensionless axial, radial, and circumferential velocity components, respectively. The dimensionless parameters in equations (1-5) are: the disk Grashof number, $\mathrm{Gr_d} = \bar{g}(\bar{\rho}_{in} - \bar{\rho}_d)\bar{r}_d^3/(\bar{\rho}_d\bar{\nu}_{in}^2)$, the spin Reynolds number, $\mathrm{Re}_\omega = \bar{r}_d^2\bar{\omega}/\bar{\nu}_{in}$, and the Prandtl number, $\mathrm{Pr} = \bar{c}_{p_{in}}\bar{\mu}_{in}/\bar{k}_{in}$ ($\bar{\omega}$ is the disk spin rate; $\bar{\nu}, \bar{\mu}, \bar{\rho}, \bar{c}_p$, and $\bar{k}$ are the kinematic and dynamic viscosities, density, specific heat at constant pressure, and thermal conductivity, respectively). The properties are normalized based on their values at the temperature at the reactor inlet, $\bar{T}_{in}$. The usual scaling (Evans and Greif, 1987) for a rotating disk has been used: $\sqrt{\bar{\omega}\,\bar{\nu}_{in}}$ for the axial component of velocity, $\bar{r}_d\,\bar{\omega}$ for the radial and circumferential components of velocity, $\sqrt{\bar{\nu}_{in}/\bar{\omega}}$ for the axial coordinate, and $\bar{r}_d$ for the radial coordinate, where symbols with overbars represent dimensional quantities. The dimensionless temperature is $T = (\bar{T} - \bar{T}_{in})/(\bar{T}_d - \bar{T}_{in})$.

The boundary conditions are:

$$
\begin{array}{lll}
x = 0 & 0 \le r \le 1 & u = v = 0, f = T = 1 \\
r = A & h - H \le x \le h & u = v = f = 0, T = \\
& & \quad -\frac{\mathrm{MCP_w}}{\mathrm{MCP_d}}(u_{in}{}^3/\mathrm{Re}_{in}) \\
r = 1 & h - H \le x \le 0 & u = v = f = \partial T/\partial r = 0 \\
r = 0 & 0 \le x \le h & \partial u/\partial r = \partial f/\partial r = \\
& & \quad \partial T/\partial r = v = 0 \\
x = h & 0 \le r \le A & v = f = T = 0, \\
& & \quad u = \mathrm{Re}_{in}/(2A\sqrt{\mathrm{Re}_\omega})
\end{array}
$$

where the inlet Reynolds number, $\mathrm{Re}_{in} = 2\bar{r}_o\bar{u}_{in}/\bar{\nu}_{in}$, $A = \bar{r}_o/\bar{r}_d$, and for an ideal gas, the disk Grashof number, $\mathrm{Gr_d} = \bar{g}(\bar{T}_d - \bar{T}_{in})\bar{r}_d^3/(\bar{T}_{in}\bar{\nu}_{in}^2)$, the wall Grashof number, $\mathrm{Gr_w} = \bar{g}(\bar{T}_{in} - \bar{T}_w)(2\bar{r}_o)^3/(\bar{T}_{in}\bar{\nu}_{in}^2)$, the disk mixed convection parameter, $\mathrm{MCP_d} = \mathrm{Gr_d}/\mathrm{Re}_\omega^{3/2}$, and the wall mixed convection parameter, $\mathrm{MCP_w} = \mathrm{Gr_w}/\mathrm{Re}_{in}{}^2$. In the current study, Re_{in} is not an independent parameter because we consider only cases where the inlet velocity is set equal to the asymptotic velocity for an infinite rotating disk: $\bar{u}_{in} = C\sqrt{\bar{\omega}\,\bar{\nu}_{in}}$, which gives $u_{in} = C$, where C is a function of the inlet temperature, $\bar{T}_{in}$, the disk temperature $\bar{T}_d$ and the gas (Evans and Greif, 1987). Thus in this study, $\mathrm{Re}_{in} = 2AC\sqrt{\mathrm{Re}_\omega}$, and the dimensionless reactor wall temperature is $T_w = -(\mathrm{MCP_w}/\mathrm{MCP_d})[C^2/(2A\sqrt{\mathrm{Re}_\omega})]$. Fully developed conditions are applied at the outflow boundary.

The equations are integrated over control volumes and discretized using the hybrid differencing scheme (Patankar, 1980). The SIMPLER method is used to determine the pressure, p_m. A sequential iterative line relaxation scheme is used to solve the equations. A more detailed description of the numerical method is given by Winters *et al.* (1996).

The results discussed here were obtained on a nonuniform grid of 80 by 40 control volumes in the x and r directions, respectively, between the inlet and the disk, with finer grid spacings near the rotating disk ($x = 0$). The control volumes were distributed over three computational regions (one bounded by the inlet and the disk, a second adjacent to the first bounded by the inlet and the beginning of the annular exit, and a third for the annular exit). A nonuniform grid of 25 by 10 control volumes in the x and r directions was used for the annular exit. Calculations made on a coarser grid resulted in disk heat flux differences of less than 5% for the two grid distributions. Furthermore, the fine grid resolution of the rotating disk boundary layer was deemed adequate because the results of the numerical calculations at the centerline ($r = 0$) differed from the similarity solution for the flow over an infinite rotating disk by less than 2%.

RESULTS AND DISCUSSION

Results for the system shown in Fig. 1 are presented using the dimensionless groups defined in the previous section. Variations in the Prandtl number, Pr, were not considered since the Prandtl numbers for common carrier gases in RDRs are nearly equal (*cf.* Table 1). This study also presents new results for the effects of variable properties by considering two common CVD gases, NH_3 and He. Results were obtained for two spin Reynolds numbers which span a range characteristic of RDRs: $\mathrm{Re}_\omega = 314.5$ and $\mathrm{Re}_\omega = 3145$. For each spin Reynolds number, $\mathrm{MCP_d}$ was increased from nearly zero to a level where significant departure from the ideal infinite rotating

disk behavior was obtained. The wall mixed convection parameter, MCP_w, was varied from -30 to $+30$; negative values are for hotter walls relative to the inlet while positive values are for cooler walls relative to the inlet.

The Ideal Reactor

One measure of reactor flow suitability is how well the disk heat flux compares to the corresponding "ideal" infinite rotating disk heat flux, $\overline{q}_{1D}$ which is defined as:

$$\overline{q}_{1D} = \left[-\overline{k} \left. \frac{\partial \overline{T}}{\partial \overline{x}} \right|_{\overline{x}=0} \right]_{1D} \qquad (6)$$

Because RDRs have finite disk diameters, deviation from the ideal flow is unavoidable at the disk edges due to two-dimensional effects. For geometries like the one shown in Fig. 1, the disk heat flux usually exceeds the ideal value at the disk edges due the local flow acceleration which accompanies the flow into the narrow exit channel. However, under stable operating conditions, it is reasonable to expect the RDR flow to approximate the ideal flow over a large portion of the disk.

Fig. 2 illustrates reactor flow (NH_3) characteristics for $Re_\omega = 314.5$, $MCP_d = 1.3$, and $MCP_w = 0$ Fig. 2(a) shows the reactor in cross-section with white streamlines superimposed over grey shaded temperature contours. Dark grey corresponds to the lowest temperature (inlet and cold walls) and light grey corresponds to the highest temperature (disk) in the flow field. A more detailed legend of contour values will not be presented because these plots are intended to demonstrate the qualitative nature of the flow even though the plots were generated from computed results. More quantitative information is presented in Fig. 2(b) which shows the heat flux distribution along the disk surface. The radial position is normalized by the disk radius (9 cm) and the heat flux is normalized by the ideal infinite rotating disk heat flux ($3.37 \times 10^6 ergs/s - cm^2$) which was computed from the similarity solution (Evans and Greif, 1988).

The normalized heat flux plot of Fig. 2(b) shows excellent agreement between the 2-D model and the 1-D result over 60% of the disk radius. Uniformity is increased to 90% when the spin Reynolds number is increased to 3145 while maintaining $MCP_d = 1.3$, and $MCP_w = 0$ (results not shown here). Increasing Re_ω also produces a thinner thermal boundary layer at the disk and correspondingly higher heat flux.

The Influences of MCP_d and Re_ω

Results were obtained for a range of MCP_d values (1.3-20) at two spin Reynolds numbers (314.5 and 3145) for NH_3 flow and $MCP_w = 0$. Fig. 3 shows reactor behavior for MCP_d values of 10 and 15 and $Re_\omega = 314.5$. Normalized disk heat flux distributions are shown in Fig. 3(c). At $MCP_d = 10$, some departure from the 1-D behavior is apparent; the magnitude has increased slightly but the distribution remains relatively uniform. At $MCP_d = 15$ there is a recirculating flow that affects both the magnitude and uniformity of the disk heat flux. Further increases in MCP_d cause stronger recirculations and correspondingly greater departure from the 1-D heat

flux result. At $Re_\omega = 3145$, departure from 1-D behavior was less pronounced (less than 5 % for $MCP_d = 15$) and no recirculations were observed but unsteady flow occurred for $MCP_d > 15$.

The Influence of MCP_w and Re_ω

In order to determine the influence of wall temperature on reactor flow and heat transfer, the wall mixed convection parameter, MCP_w, was varied over a range typical for RDRs. The disk mixed convection parameter, MCP_d was fixed at 5 and results were obtained for NH_3 at the two spin Reynolds numbers (314.5 and 3145). Fig. 4 shows reactor flow and temperature for $MCP_w = -30, 0, +30$ and $Re_\omega = 314.5$. The corresponding disk heat flux profiles are shown in Fig. 5. For $MCP_w = -30$, the wall is hotter than the downward flowing gas, and a buoyancy induced recirculation develops near the reactor walls. This causes the downward flow to be channeled inward toward the reactor centerline; note the inward curvature of the streamlines in Fig. 4(a). This results in a slight increase in the disk heat transfer over the entire disk. Cooling the walls relative to the inlet ($MCP_w = +30$) causes a downward sidewall flow that leads to a weak recirculation and reduced heat flux over the outer half of the disk. Similar calculations performed for $Re_\omega = 3145$ also exhibited flow recirculations but departure from 1-D heat flux behaviour was less as shown in Fig. 6.

At higher values of MCP_d, variations in MCP_w lead to greater departures from the 1-D behavior. Fig. 7 and Fig. 8 show results for MCP_w of $-30, 0, +30$ at $MCP_d = 7$ and $Re_\omega = 3145$. The small increase in MCP_d from 5 to 7 results in a substantial increase in disk heat flux nonuniformity. Further increases in MCP_d lead to unsteady flows for $MCP_w = +30$.

The Influence of Variable Gas Properties

Table 1 shows transport property and Prandtl number variations for common RDR gases evaluated at 400 and 1300 K. Prandtl numbers for the common carrier gases are nearly equal and constant over the temperature range considered here. Hence, if it could be shown that variations of the transport properties with temperature are unimportant, the results presented in the previous sections would apply for all the common carrier gases.

To determine the influence of variable transport properties, several calculations were repeated using He in place of NH_3. Note that the largest variation in transport properties for the gases shown in Table 1 occurs for NH_3, the least for He. Fig. 9 shows flow fields and disk heat flux profiles for He and NH_3 for $Re_\omega = 314.5$, $MCP_w = 0$ and $MCP_d = 15$. Using the asymptotic velocity caused Re_{in} for the NH_3 and He calculations to be slightly different (47 for NH_3 and 42 for He). NH_3 flow exhibits significant departure from 1-D flow with nonuniform heat transfer and strong recirculating flow. In contrast, the He flow resembles the 1-D result with only a slight nonuniformity in the disk heat flux. At $MCP_d \leq 10$ both gases exhibit 1-D behavior (results not shown here).

CONCLUSIONS

The results for NH_3 show that increasing Re_ω from 314.5 to 3145 increases the uniformity of the rotating disk heat flux and results in thinner thermal boundary layers at the disk surface. At $Re_\omega = 314.5$, increasing MCP_d to 15 leads to significant departure from the 1-D infinite disk result with nonuniform disk heat fluxes and recirculating flow patterns; the flow becomes increasingly complex at larger values of MCP_d. At the larger value of Re_ω of 3145, the results are closer to the 1-D infinite disk for MCP_d up to 15.

For large negative (hot walls) and positive (cold walls) values of MCP_w, the flow recirculates and there is significant deviation from the one-dimensional result; the nonuniformities occur at $Re_\omega = 314.5$ and 3145. The sensitivity to large variations in MCP_w is increased at larger MCP_d and lower Re_ω. Substituting He for NH_3 for several calculations demonstrated the strong influence due to the variable transport properties. For He (smaller variation in transport properties), the disk thermal boundary layers tended to be thinner and the flow was more stable over a larger range of MCP_d.

NOMENCLATURE

A	radial aspect ratio, $\bar{r}_o/\bar{r}_d$
C	nondimensional asymptotic velocity for the infinite rotating disk (.88 for NH_3 and .79 for He; $\bar{T}_{in}=400K$, $\bar{T}_d=1300K$)
$Gr_d/Re_\omega{}^{3/2}$	disk mixed convection parameter, $MCP_d = \bar{g}(\bar{T}_d - \bar{T}_{in})/(\bar{T}_{in}\bar{\nu}_{in}^{1/2}\bar{\omega}^{3/2})$
$Gr_w/Re_{in}{}^2$	wall mixed convection parameter, $MCP_w = \bar{g}(\bar{T}_{in} - \bar{T}_w)\cdot 2\bar{r}_o/(\bar{T}_{in}\bar{u}_{in}^2)$
P	pressure
Pr	Prandtl number, $\bar{c}_{p_{in}}\bar{\mu}_{in}/\bar{k}_{in}$
$\bar{q}_{1D}$	1-D infinite rotating disk heat flux
Re_ω	spin Reynolds number, $\bar{r}_d{}^2\bar{\omega}/\bar{\nu}_{in}$
Re_{in}	inlet Reynolds number, $2\bar{r}_o\bar{u}_{in}/\bar{\nu}_{in} = 2AC\sqrt{Re_\omega}$
T	temperature
c_p	specific heat at constant pressure
f	ratio w/r
$\bar{g}$	acceleration of gravity (dimensional)
h	disk to inlet height
k	thermal conductivity
p_m	pressure in momentum equations
r	radial coordinate
$\bar{r}_o$	reactor radius (dimensional)
u	axial velocity component
v	radial velocity component
w	circumferential velocity component
x	axial coordinate

Greek Symbols

ρ	density
ν	kinematic viscosity
μ	dynamic viscosity
ω	disk spin rate

Superscripts and Subscripts

d	disk quantity
w	reactor wall quantity (for $h - H \leq x \leq h, r = A$)
$^-$	dimensional quantity
in	evaluated at reactor inlet, reference conditions
1D	one-dimensional value

REFERENCES

Evans, G.H. and Greif, R., 1987, A Numerical Model of the Flow and Heat Transfer in a Rotating Disk Chemical Vapor Deposition Reactor, in *J. Heat Transfer*, vol. 109, pp.928-935.

Patnaik, S., Brown, R.A., and Wang, C.A., 1989, Hydrodynamic Dispersion in Rotating Disk OMVPE Reactors, in *J. Crystal Growth*, vol. 96, pp.153-174.

Chou, F. and Gong, S., 1994, Effect of Wall Cooling on the Flow Regime Map in a Rotating-Disk CVD Reactor, in *J. Chemical Vapor Deposition*, vol. 3, pp.47-64.

Palmateer, S.C., Groves, S.H., Wang, C.A., Weyburne, D.W. and Brown, R.A., 1987, Use of Flow Visualization and Tracer Gas Studies for designing an INP/InGaAsP OMVPE Reactor, in *J. Crystal Growth*, vol. 83, pp.202-210.

Winters, W.S., Evans, G.H. and Greif, R., 1997, Mixed Binary Convection in a Rotating Disk Chemical Vapor Depositon Reactor, in *Int. J. Heat Mass Transfer*, vol. 40, pp.737-744.

Evans, G.H. and Greif, R., 1988, Forced Flow Near a Heated Rotating Disk: A Similarity Solution, in *Num. Heat Transfer*, vol. 14, pp.373-387.

Patankar, S.V., 1980, *Numerical Heat Transfer and Fluid Flow*, McGraw-Hill, New York.

Winters, W.S., Evans, G.H., and Moen, C.D., 1996, CURRENT - A Computer Code for Modeling Two-Dimensional, Chemically Reacting, Low Mach Number Flows, SAND97-8202 Report, October.

Carrier Gas	$\dfrac{k_{1300}}{k_{400}}$	$\dfrac{\mu_{1300}}{\mu_{400}}$	Pr_{400}	Pr_{1300}
NH_3	4.75	2.99	.72	.73
H_2	2.35	2.15	.69	.69
He	2.14	2.15	.67	.67
N_2	2.58	2.21	.71	.71
O_2	2.64	2.23	.71	.71
Ar	2.28	2.28	.67	.67

Table 1: Carrier gas properties at 400K and 1300K.

$\bar{r}_o$

Uniform Inlet Flow, $\bar{u}_{in}$

$\bar{r}_o = 13.5$ cm
$\bar{r}_d = 9$ cm
$\bar{h} = 18$ cm
$\bar{H} = 28$ cm

Rotating Disk Surface

X

r

$\bar{r}_d$

Exit Flow

Exit Flow

$\bar{h}$

$\bar{H}$

Figure 1: Reactor Geometry.

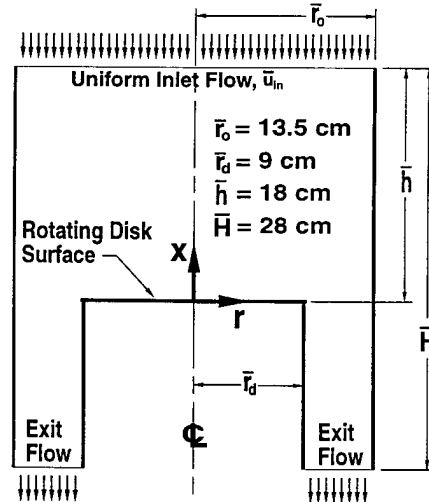(a) Grey fill temperature contours with superimposed streamlines.
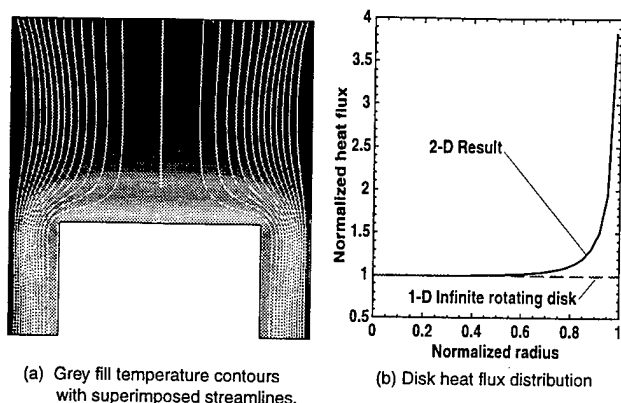
(b) Disk heat flux distribution

Figure 2: Comparison with 1-D infinite rotating disk solution for $Re_\omega = 314.5$, $MCP_d = 1.3$, and $MCP_w = 0$. Conditions: 13.5 torr, 562 RPM, $\overline{T}_d = 1300K$, $\overline{T}_{in} = 400K$, $\overline{T}_w = 400K$, $-\overline{u}_{in} = 26.3cm/sec$, and $\overline{q}_{1D} = 3.37 \times 10^6 ergs/sec - cm^2$.

(a) Disk MCP=10

(b) Disk MCP=15

(c) Disk heat flux

Figure 3: Influence of MCP_d on flow and temperature at $Re_\omega = 314.5$. Conditions: $\overline{T}_d = 1300, K$, $\overline{T}_{in} = 400K$, $\overline{T}_w = 400K$, and $\overline{q}_{1D} = 3.37 \times 10^6 ergs/sec - cm^2$; (a) 38 torr, 198 RPM, $-\overline{u}_{in} = 9.3cm/sec$, (b) 47 torr, 162 RPM, $-\overline{u}_{in} = 7.6cm/sec$, (c) Disk heat flux distributions for 4 values of MCP_d.

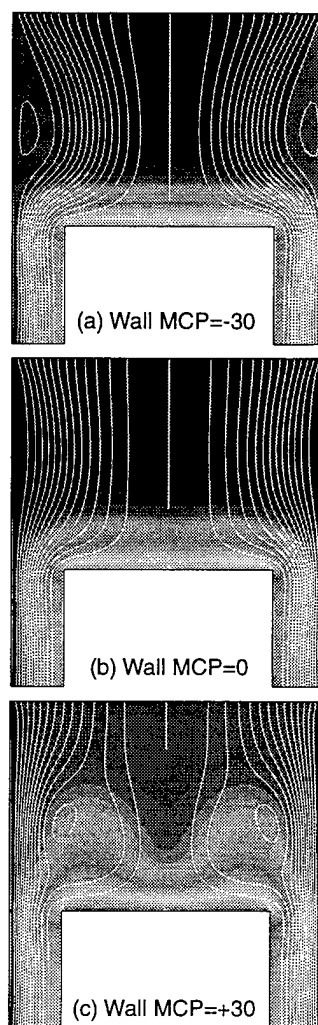(a) Wall MCP=-30

(b) Wall MCP=0

(c) Wall MCP=+30

Figure 4: Influence of MCP_w on flow and temperature at $Re_\omega = 314.5$ and $MCP_d = 5$. Conditions: 27 torr, 281 RPM, $-\overline{u}_{in} = 13.2cm/sec$, $\overline{T}_d = 1300K$, $\overline{T}_{in} = 400K$, and $\overline{q}_{1D} = 3.37 \times 10^6 ergs/sec - cm^2$; (a) $\overline{T}_w = 479K$, (b) $\overline{T}_w = 400K$, (c) $\overline{T}_w = 321K$.
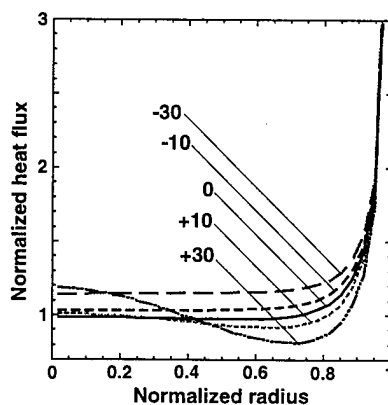

Figure 5: Influence of MCP_w on disk heat flux at $Re_\omega = 314.5$ and $MCP_d = 5$. Conditions: 27 torr, 281 RPM, $-\overline{u}_{in} = 13.2cm/sec$, $\overline{T}_d = 1300K$, $\overline{T}_{in} = 400K$, and $\overline{q}_{1D} = 3.37 \times 10^6 ergs/sec - cm^2$; $MCP_w = -30$: $\overline{T}_w = 479K$, $MCP_w = -10$: $\overline{T}_w = 426K$, $MCP_w = 0$: $\overline{T}_w = 400K$, $MCP_w = +10$: $\overline{T}_w = 374K$ $MCP_w = +30$: $\overline{T}_w = 321K$.
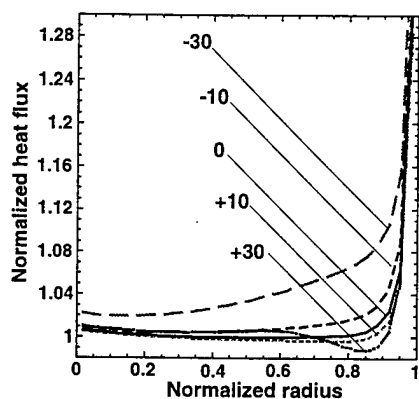
Figure 6: Influence of MCP_w on disk heat flux at $Re_\omega = 3145$ and $MCP_d = 5$. Conditions: 152 torr, 500 RPM, $-\overline{u}_{in} = 7.4$cm/sec, $\overline{T}_d = 1300$K, $\overline{T}_{in} = 400$K, and $\overline{q}_{1D} = 1.07 \times 10^7$ergs/sec $-$ cm^2; $MCP_w = -30$: $\overline{T}_w = 424$K, $MCP_w = -10$: $\overline{T}_w = 406$K, $MCP_w = 0$: $\overline{T}_w = 400$K, $MCP_w = +10$: $\overline{T}_w = 392$K, $MCP_w = +30$: $\overline{T}_w = 376$K.

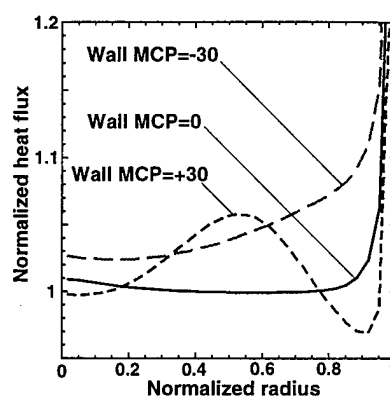Figure 8: Heat flux influence of MCP_w at $Re_\omega = 3145$ and $MCP_d = 7$. Conditions: 180 torr, 423 RPM, $-\overline{u}_{in} = 6.3$cm/sec, $\overline{T}_d = 1300$K, $\overline{T}_{in} = 400$K, and $\overline{q}_{1D} = 1.07 \times 10^7$ergs/sec $-$ cm^2.

(a) Ammonia

(b) Helium

(c) Disk MCP=15

Figure 9: Influence of transport properties at $Re_\omega = 314.5$ for $MCP_w = 0$ and $MCP_d = 15$. NH$_3$ conditions: 46.7 torr, 162 RPM, $-\overline{u}_{in} = 7.6$cm/sec, $\overline{T}_d = 1300$K, $\overline{T}_{in} = 400$K, $\overline{T}_w = 400$K and $\overline{q}_{1D} = 3.37 \times 10^6$ergs/sec $-$ cm^2; He conditions: 277 torr, 163 RPM, $-\overline{u}_{in} = 6.8$cm/sec, $\overline{T}_d = 1300$K, $\overline{T}_{in} = 400$K, $\overline{T}_w = 400$K and $\overline{q}_{1D} = 8.79 \times 10^6$ergs/sec $-$ cm^2 .

(a) Wall MCP=-30
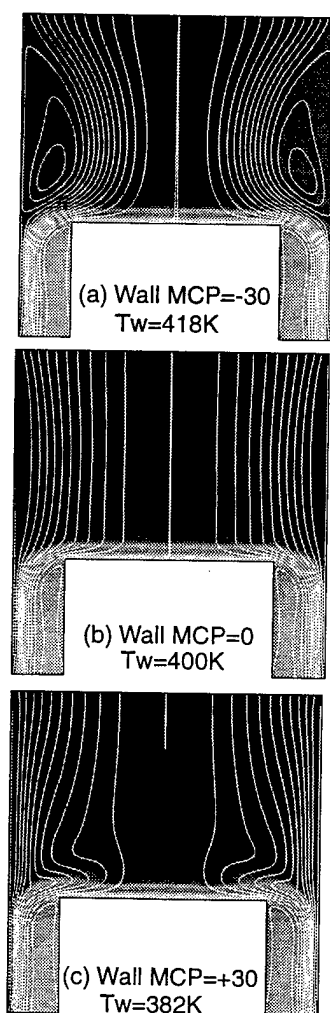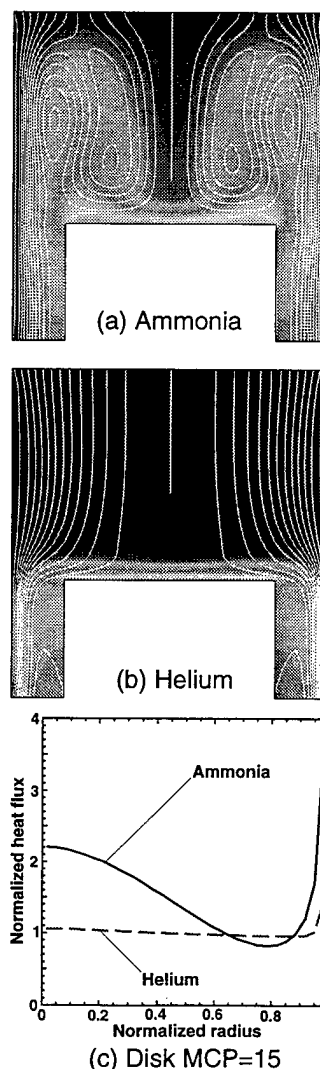Tw=418K

(b) Wall MCP=0
Tw=400K

(c) Wall MCP=+30
Tw=382K

Figure 7: Flow field influence of MCP_w at $Re_\omega = 3145$ and $MCP_d = 7$. Conditions: 180 torr, 423 RPM, $-\overline{u}_{in} = 6.3$cm/sec, $\overline{T}_d = 1300$K, $\overline{T}_{in} = 400$K, and $\overline{q}_{1D} = 1.07 \times 10^7$ergs/sec $-$ cm^2.

Report Number (14) _SAND--98-8482C_
CONF-980506

Publ. Date (11) _199808_
Sponsor Code (18) _DOE/EE , XF_
UC Category (19) _UC-1409 , DOE/ER_

19980707 078

DOE